A Highly Ordered Meso@Microporous Carbon-Supported Sulfur@Smaller Sulfur Core–Shell Structured Cathode for Li–S Batteries

Zhen Li,[†] Yan Jiang,[†,‡] Lixia Yuan,[†,*] Ziqi Yi,[†] Chao Wu,[†] Yang Liu,[†] Peter Strasser,[§] and Yunhui Huang[†,*]

[†]State Key Laboratory of Material Processing and Die & Mold Technology, School of Materials Science and Engineering, Huazhong University of Science and Technology, Wuhan, Hubei 430074, China, [‡]School of Electrical & Electronic Engineering, Hubei University of Technology, Wuhan, Hubei 430068, China, and [§]The Electrochemical Energy, Catalysis, and Materials Science Laboratory, Department of Chemistry, Chemical Engineering Division, Technical University Berlin, Berlin 10623, Germany

ABSTRACT For lithium–sulfur batteries, commercial application is hindered by the insulating nature of sulfur and the dissolution of the reaction intermediates of polysulfides. Here, we present an ordered meso-microporous core–shell carbon (MMCS) as a sulfur container, which combines the advantages of both mesoporous and microporous carbon. With large pore volume and highly ordered porous structure, the "core" promises a sufficient sulfur loading and a high utilization of the active material, while the "shell" containing microporous carbon and smaller sulfur acts as a physical barrier and stabilizes the cycle capability of the entire S/C composite. Such a S/MMCS composite exhibits a capacity as high as 837 mAh g^{-1} at 0.5 C after 200 cycles with a capacity retention of 80% vs the second cycle (a decay of only 0.1% per cycle), demonstrating that the diffusion of the polysulfides into the bulk electrolyte can be greatly reduced. We believe that the tailored highly ordered meso-microporous core–shell structured carbon can also be applicable for designing some other electrode materials for energy storage.

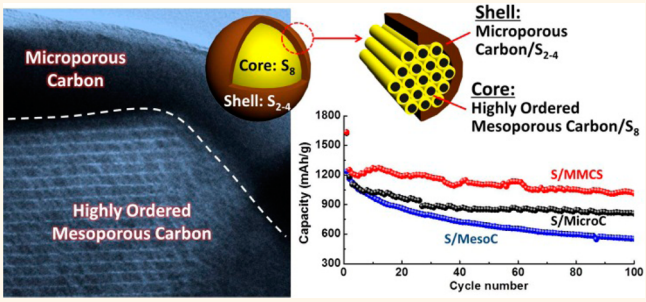

KEYWORDS: highly ordered meso-microporous carbon · core–shell structure · Li–S batteries · electrochemical performance · smaller sulfur molecules

The lithium–sulfur (Li–S) rechargeable battery has a theoretical energy density as high as 2600 Wh kg^{-1}, promising a revolutionary advantage as the next-generation energy storage system. However, the realization of practical application is still hindered by the low capacity release of S and the severe capacity fading over cycling.[1−4] The low sulfur utilization is generally caused by the insulating nature of S (5×10^{-28} S m^{-1}), while the poor cycle stability is mainly due to the high dissolubility of the reaction intermediates of lithium polysulfides (Li_2S_x, $4 < x \leq 8$).[5−7]

In order to overcome the hurdles in Li–S battery technology, various approaches have been proposed to enhance the actual capacity and the cycle stability of the sulfur cathode.[8−18] Among them, the most widely used method is to compose sulfur with various carbon matrices, which can interact with various atoms, ions, molecules, or even larger guest species through the whole internal porous system.[19−21] Because of the close contact between sulfur and conductive host and the sorption property of the nanostructured carbon, the electronic conductivity of the sulfur composite is greatly enhanced, and the diffusion of the dissolved polysulfides in the electrolyte is also suppressed effectively, leading to a remarkably improved sulfur utilization and cycle stability. The pioneering work was carried out by Nazar's group in 2009,[22] in which a typical ordered mesoporous carbon, CMK-3, was used to encapsulate sulfur molecules to improve the utilization of active material and restrain the shuttle effect caused by the polysulfide species. After that, various carbonaceous materials have been investigated as the conducting and confining hosts, such as ordered/disordered mesoporous,[22−24]

* Correspondence to huangyh@hust.edu.cn, yuanlixia@hust.edu.cn.

Received for review June 14, 2014 and accepted August 21, 2014.

Published online August 21, 2014
10.1021/nn503220h

© 2014 American Chemical Society

microporous carbon,[25−27] hollow carbon spheres,[28−30] carbon nanofibers,[31−34] graphenes,[35−38] and some composites of the above structures.[39−43]

In general, to achieve an ideal electrochemical performance, the carbon host for the sulfur composite should meet the following requirements: (1) high electrical conductivity to ensure an efficient conductive network in the sulfur cathode; (2) large pore volume to obtain a high maximum sulfur loading; (3) hierarchical interconnected micro/mesopores to accommodate the sulfur species and suppress the diffusion of the dissolved polysulfides to the bulk electrolyte, and meanwhile to favor the infiltration of the electrolyte to ensure fast transport of Li ions during the redox process; (4) robust mechanical properties to endure the volumetric change of the electrode during the lithiation/delithiation reaction. Although many kinds of carbonaceous materials have been designed to confine sulfur species, no one can completely meet all the above requirements. Some contradictions always exist between the energy density and the electrochemical performance. For example, many S/C composites show a very high specific capacity (>1000 mAh g^{-1}), but most of them usually provide a low sulfur content.[42,44−46] The higher the sulfur utilization, the lower the sulfur content is. A similar inconsistency also happens between the sulfur loading and the cycle stability. Low sulfur content greatly reduces the overall volumetric capacity and energy density of the cathode. It seems that a simply structured carbon host cannot bring both high sulfur loading and good electrochemical performance.

Mesoporous carbon is widely used as sulfur host. It can afford a high sulfur loading, but the cycle stability is always poor because the S nanofillers in mesopores are still accessed by organic liquid electrolyte solvents so that the dissolution cannot be suppressed effectively, especially during long cycles.[13,47] Some polymers have been used as surface coating layers to restrain the dissolution of the polysulfides.[48−50] However, the improvement of cyclability in the polymer@S/C composites reported is not sufficient enough for application. Moreover, most of the additional polymer coatings are electrochemically inert, which reduce the overall volumetric capacity and energy density of the sulfur cathode. Using microporous carbon as sulfur supporter is helpful to get an impressive cycling stability. Guo *et al.* have proved that, if the pore size is less than 0.5 nm, sulfur exists as smaller chainlike S_{2-4} molecules due to the space limitation.[26] Thus, the higher order polysulfides that can dissolve into the electrolyte would not be formed during discharging−charging process. Although the sulfur composite cathode based on microporous carbon gives a significantly improved cycling stability, the sulfur loading is always limited (~40 wt %), and the discharging plateaus is low (~1.85 V) due to the "solid−solid" process,[44] leading to a relatively lower energy density of the S/C composites. Therefore, neither mesoporous carbon nor microporous carbon can afford an ideal sulfur cathode separately. If we combine these two kinds of carbons together to fabricate a hierarchical nanoarchitecture, their individual intrinsic advantages can be taken perfectly.

Here, we demonstrate a hybrid nanoarchitecture with highly ordered meso-microporous core−shell carbon (MMCS) as sulfur container. Such a core−shell-structured carbon inherits the natures of both mesoporous carbon (mesoC) and microporous carbon (microC), showing a large pore volume and highly ordered porous structure. The "core" promises a sufficient sulfur loading and a high utilization of the active material; the "shell" not only acts as a physical barrier to stabilize the cycle life but also enhances the rate capability of the whole composite cathode.

RESULTS AND DISCUSSION

The synthesis process of MMCS is illustrated in Figure 1a. Previous studies have proven that sulfur particles can be filled into the micropores readily *via* the melting−diffusion route.[25,26] Here we presume that, in the liquid state, sulfur can penetrate into the inner mesopores through the outer microporous shell. During the cooling process, the liquid sulfur solidifies and then is confined into the inner mesopores at room temperature. Figure 1b demonstrates the structural advantages of the S/MMCS composite. The microporous carbon shell loads smaller S_{2-4} molecules and acts as a strong barrier to suppress the diffusion of the dissolved polysulfides from "core" to bulk electrolyte. The S_{2-4} molecules are much more stable than S_8 during cycling.

Transmission electron microscopy (TEM) and high-resolution TEM (HRTEM) images of MMCS are shown in Figure 2a−c. Unlike the traditional mesoC (Figure 2d,e), an additional carbon shell with a thickness of 80−100 nm can be clearly identified as dark sheath on the MMCS particles (marked in Figure 2a), showing a microporous structure (Figure 2c). Since molecular sieve SBA-15 was applied as hard template, the mesoporous core of MMCS has the same highly ordered structure as CMK-3, which can be clearly observed in Figure 2b. The small-angle X-ray diffraction (SAXRD) patterns (Figure 2f) also verify the inner highly ordered structure of MMCS. A joint curve of types I and IV nitrogen adsorption/desorption isotherms further confirm the micromesoporous hybrid structure of MMCS (Figure S1, Supporting Information), consistent with the TEM observations. The calculated Brunauer−Emmett−Teller (BET) surface area and total pore volume are 1013 $m^2 g^{-1}$ and 1.26 $cm^3 g^{-1}$, respectively. The theoretical maximum loading of sulfur is 72 wt % based on the density of S (2.07 g cm^{-3}).

Pure microC and mesoC were synthesized for comparison. All of the carbon samples were attained with

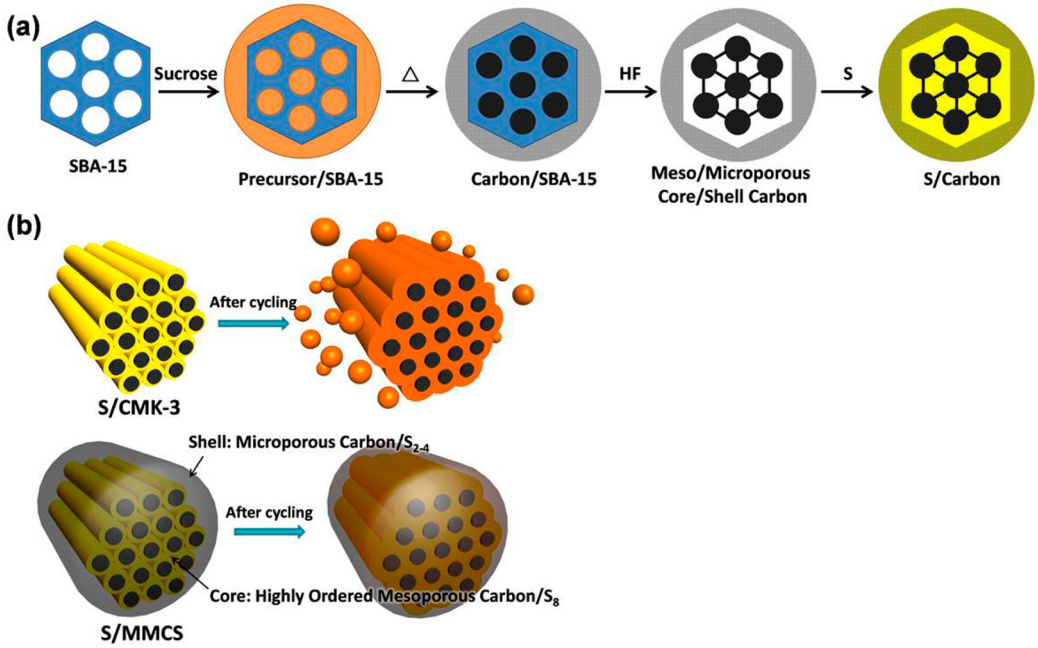

Figure 1. (a) Schematic for preparation of highly ordered meso-microporous core−shell (MMCS) carbon and sulfur/carbon composite. (b) Schematic of the mesoC/S_8-microC/S_{2-4} core−shell structure.

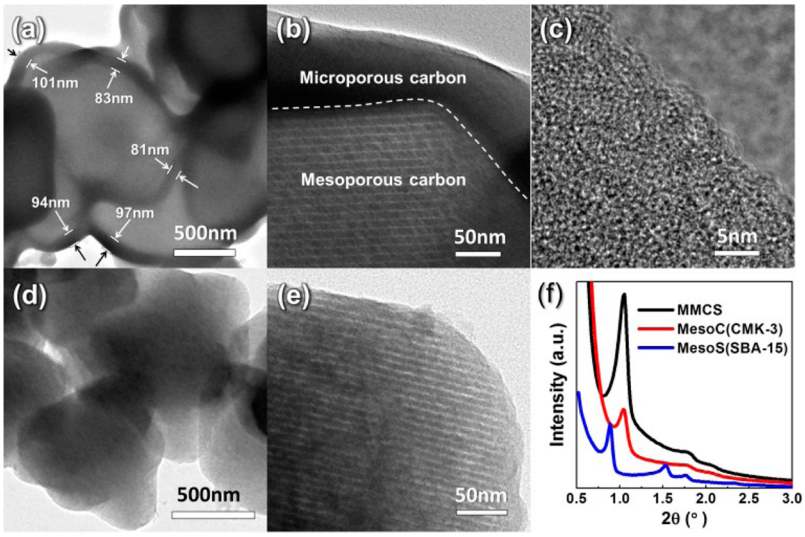

Figure 2. TEM and HRTEM images of (a−c) MMCS and (d, e) mesoC. (f) SAXRD patterns of MMCS, mesoC (CMK-3) and mesoporous SiO_2 (SBA-15).

the same precursor and carbonization temperature to ensure that they have almost same degree of graphitization, which has been proved by XRD and Raman results (Figure S2, Supporting Information). Therefore, the electrochemical performances of the S/C composites should be mainly determined by the characteristic of the carbon structures. Parts a−c of Figure 3 show typical scanning electron microscopy (SEM) images of mircoC, mesoC, and MMCS. The microC spheres are of about 1 μm in size with a smooth surface. For mesoC, the porous structure can be clearly observed from the exposed surface. From a broken particle of MMCS, we can see that the designed microporous shell surrounds the mesoporous core (Figure 3c). The XRD patterns of the S/microC, S/mesoC, and S/MMCS composites are shown in Figure S3 (Supporting Information). No sulfur diffraction peaks are observed in all three samples, indicating that S particles are well confined within the carbon structures. Parts d−f of Figure 3 show the SEM images of the three composites. Both S/microC and S/MMCS resemble the particles before sulfur loading. The S/mesoC shows a smooth surface after sulfur loading, indicating that the sulfur particles are well filled into the mesopores. Determined by thermogravimetric analysis (TGA), the S contents are 30.1, 65.8, and 60.6 wt % for S/microC, S/mesoC, and S/MMCS,

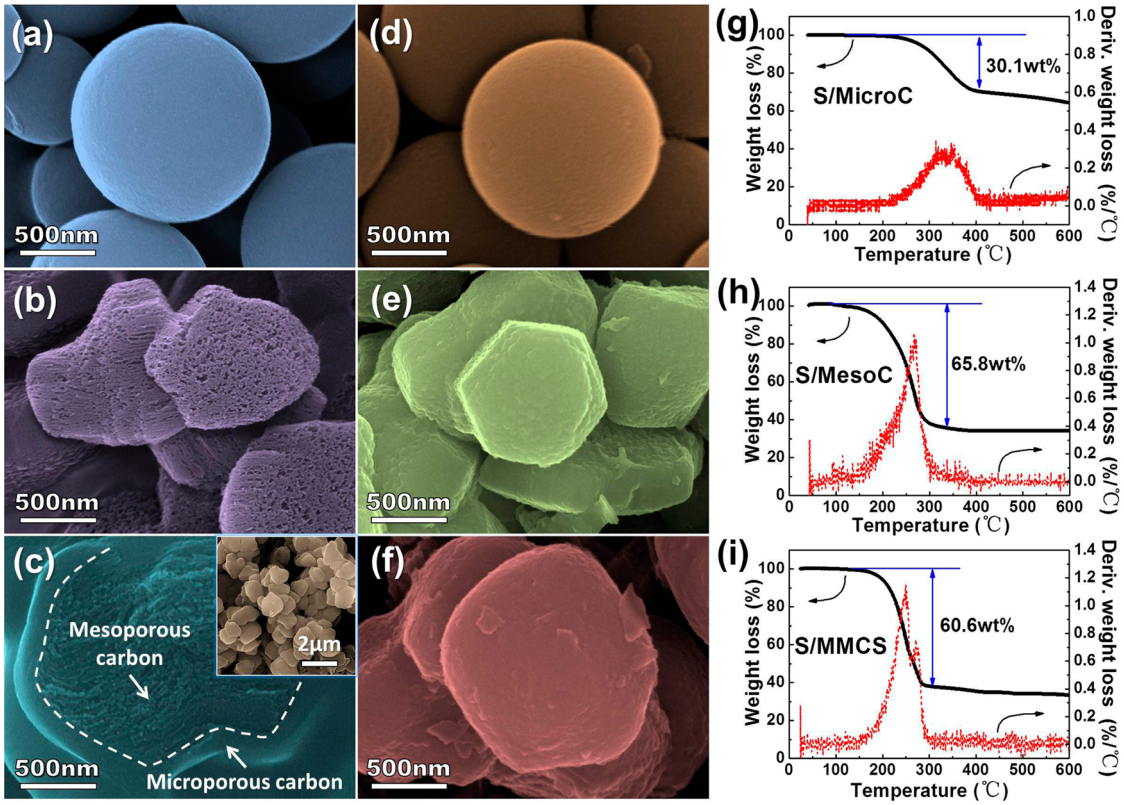

Figure 3. SEM images of (a) microC, (b) mesoC, (c) MMCS, (d) S/microC, (e) S/mesoC, and (f) S/MMCS. TG curves of (g) S/microC, (h) S/mesoC, and (i) S/MMCS.

respectively (Figure 3g–i. S/microC has a higher sulfur-vaporizing temperature than S/mesoC because the interaction between the carbon matrix and sulfur in the micropores is stronger than that in the mesopores. For S/MMCS, the sulfur evaporation shows two steps, corresponding to the S-confining process within meso- and micropores.

The distribution of sulfur in S/MMCS was further verified by TEM and energy-dispersive X-ray spectroscopy (EDX). The TEM images (Figure 4a,b) reveal that S/MMCS still maintains the core–shell structure, but the contrast of the image becomes darker due to the sulfur impregnation. As shown in Figure 4c,d, the linear EDX elemental distributions of S and C confirm that (1) MMCS has a well-fabricated core–shell structure, in which the microporous shell has a higher density of carbon than the inner mesoporous core, and (2) the distribution of S is contrary to C, *i.e.*, the mesoporous core contains more sulfur than the outside shell. a typical SEM image of the S/MMCS electrode film is shown in Figure S4 (Supporting Information). We can see that the particles after milling and roll pressing still keep almost the same morphology as the as-prepared sample, indicating that the microporous carbon shell is mechanically rigid enough to avoid breakage.

To accurately evaluate the influence of the carbon microstructure on the electrochemical behavior of sulfur, the S/microC, S/mesoC, and S/MMCS electrode

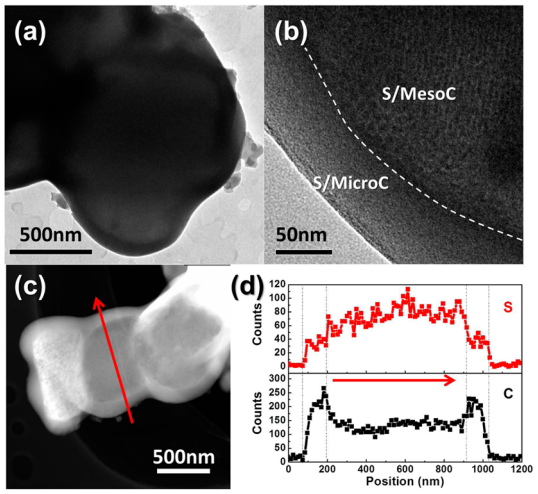

Figure 4. (a, b) TEM images and (c) dark field TEM image of S/MMCS; (d) the linear EDX element distributions of S and C along the arrow line of (c).

films were made by the same process. Considering that the activation phenomenon always appears in the first cycle, we chose the second cycle voltammetry (CV) curves of the S/microC, S/mesoC and S/MMCS cathodes for comparison to reveal the stable redox behaviors of the electrode materials (Figure 5a–c). Both S/microC and S/mesoC show their typical electrochemical features, which are similar to the previous studies:[25,50]

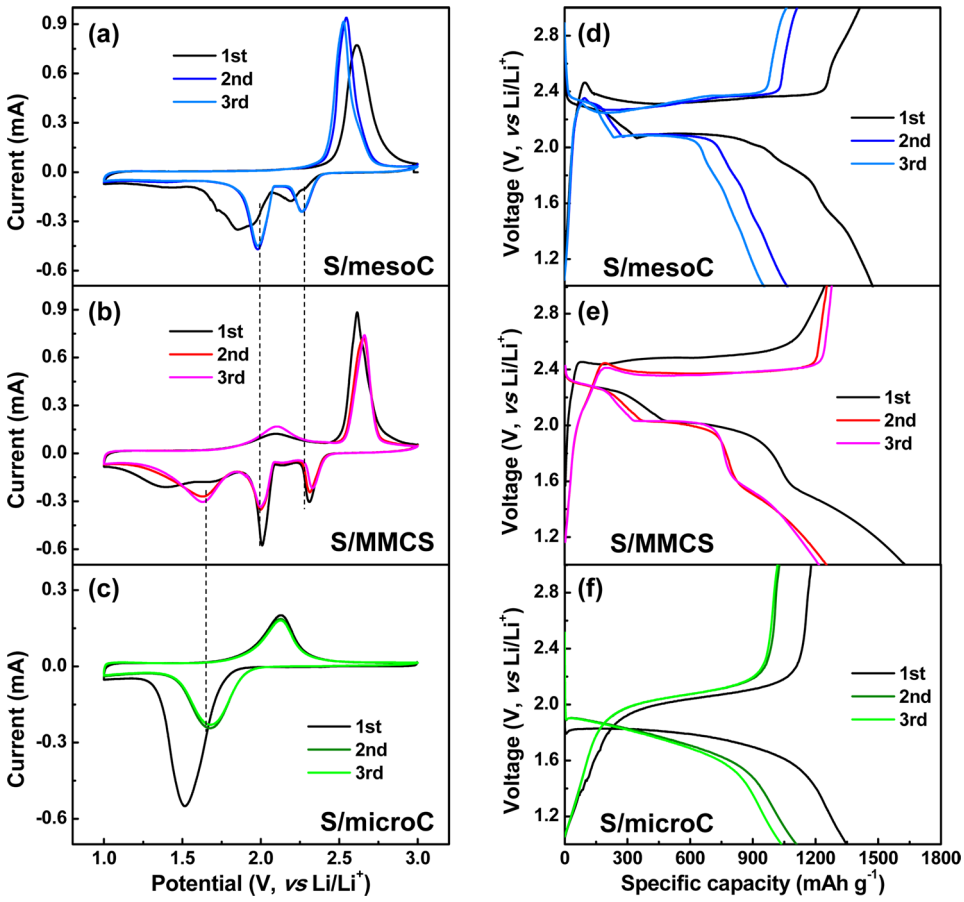

Figure 5. Comparison of the CV curves and voltage profiles at 0.2 C of (a, d) S/mesoC, (b, e) S/MMCS and (c, f) S/microC in the voltage range of 3.0−1.0 V vs Li^+/Li.

at a voltage of 3.0−1.0 V, S/microC shows a pair of wide redox peaks, while S/mesoC shows two reductive peaks and one oxidative peak, and there is no obvious reduction peaks in the voltage region of 1.5−1.0 V. For S/MMCS, it is interesting that three peaks appear at about 2.3, 2.0, and 1.7 V (vs Li^+/Li) in the cathodic reduction process. The two peaks at 2.3 and 2.0 V correspond to the reduction of S_8 molecule in the mesoporous core from S_8 to higher order polysulfides (Li_2S_x, $4 < x < 8$) and then to lower order lithium sulfides (such as Li_2S_2, Li_2S). The 1.7 V peak is related to the reduction of smaller sulfur molecules confined within the microporous shell (from S_{2-4} to Li_2S_2/Li_2S). Because of the solid−solid process, the transformations from S_{2-4} to Li_2S_{2-4} and from Li_2S_{2-4} to Li_2S_2/Li_2S cannot be separated clearly in the CV curves, and the resistance of the "solid−solid" process is relatively higher.[47] Thereby, the "solid−solid" electrochemical reactions from S_{2-4} to Li_2S_{2-4} and from Li_2S_{2-4} to Li_2S_2/Li_2S in the micropores show as a single reduction peak at a lower potential (1.7 V) in the CV curves. In the subsequent anodic process, two oxidation peaks are observed at 2.1 and 2.6 V, which are attributed to the conversion of lithium sulfides to sulfur in micropores and mesopores, respectively. The typical redox peaks of S/mesoC, S/MMCS, and S/microC are all in agreement with their own galvanostatic charge−discharge curves (Figure 5d−f). S/MMCS has three discharge plateaus, corresponding to the lithiation processes of sulfur in mesopores and micropores, respectively.

Figure 6a shows the cyclability for the three kinds of C/S cathodes. Different cycle behaviors evidently demonstrate the structural advantage of the meso-micropore core−shell carbon for sulfur capture. After the initial two cycles of activation and stabilization, the discharge capacities in the third cycle are 1123 (739), 1071 (322), and 1212 (734) mAh g^{-1} for S/mesoC, S/microC, and S/MMCS, respectively (the normal capacity values are calculated on the sulfur mass; the ones in parentheses are based on the total mass of the S/C composite). Considering the total capacity of the composite is more important for the energy density, S/mesoC and S/MMCS, with higher S loadings and higher overall capacities, are more attractive than S/microC for practical applications. But after 100 cycles, the capacity of S/mesoC decreases to 552 (363) mAh g^{-1}, which is only 49% of that in the third cycle, indicative of a high dissolution of polysulfides. On the contrary, the cycle stability of S/MMCS is almost as good as S/microC; it maintains a high capacity of 1014 (615) mAh g^{-1} after 100 cycles, about 80% capacity retention vs the third cycle. Even cycled at a higher current density of 0.5 C, the S/MMCS cathode delivers a capacity of 1037 (627) mAh g^{-1} at the

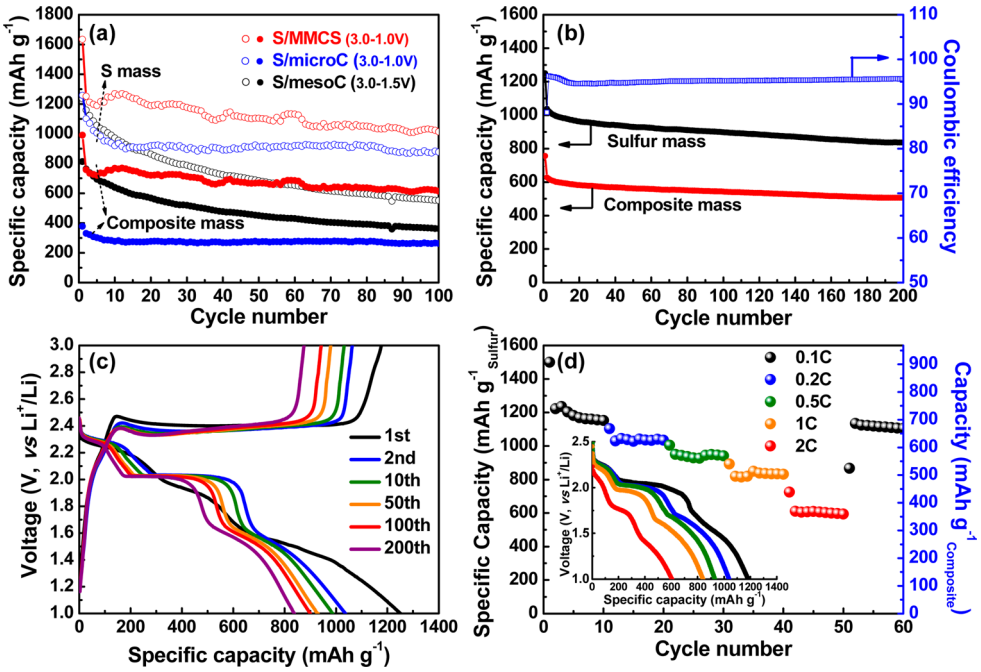

Figure 6. (a) Cycle performances of S/MMCS, S/mesoC, and S/microC at 0.1 C, (b) ,ycle performance, (c) voltage profiles during cycling at 0.5 C, and (d) rate capacities at various C-rates of S/MMCS in the voltage range of 3.0−1.0 V vs Li^+/Li. Inset of (d) shows the discharge voltage profiles at the current densities from 0.1 to 2 C.

second cycle and maintains 837 (506) mAh g^{-1} after 200 cycles with capacity retention of ~81% (a decay of 0.1% per cycle) and high coulombic efficiency up to 95%. The high capacity retention and coulombic efficiency in S/MMCS suggest that the microporous carbon shell plays an important role in retarding polysulfide dissolution. What's more, the carbon shell may also increase the reaction kinetics between lithium and sulfur. Figure 6d presents the rate capability of S/MMCS. The cell made from S/MMCS shows a discharge capacity of 1182 (715), 1038 (628), 930 (563), 840 (508), and 605 (366) mAh g^{-1} at 0.1, 0.2, 0.5, 1, and 2 C, respectively. When the current density is tuned back to 0.1 C, a reversible capacity of 1105 (669) mAh g^{-1} is achieved, indicative of good rate performance and high stability. The inset of Figure 6d shows the typical discharge profiles of S/MMCS at various current densities from 0.1 to 2 C in the potential range of 3.0−1.0 V. Three plateaus are observed in the discharge curves, corresponding to the typical electrochemical behaviors of S_8/mesoC and S_{2-4}/microC composites.

To further understand the electrode reaction mechanism of the high-performance S/MMCS electrode, we performed X-ray photoelectron spectroscopy (XPS) and analyzed the S 2p spectra of the as-prepared S/mesoC and S/MMCS samples. In Figure 7a,b, the XPS results show that sulfur molecules confined within mesopores and micropores have different chemical status. The characteristic S 2p peaks of S/mesoC are in good agreement with S_8 molecules. For S/MMCS, the outer shell of S/microC shows two more peaks at 168.2 and 169.1 eV, revealing the existence of smaller S_{2-4} molecules in the microporous carbon shell.[47] Different from S/mesoC that exhibits a "solid-liquid-solid" reaction mechanism, S/microC shows a "solid−solid" reaction mechanism with no any soluble polysulfides generated,[26,51] as seen in Figure 7c,d. Therefore, if S/microC is employed as the physical barrier outside the S/mesoC, the soluble polysulfides can be totally enclosed within the carbon matrices, and hence, the cycle stability is greatly improved. Figure S5 (Supporting Information) compares the digital photos of the cathode electrode films and Li metal electrodes of S/mesoC, S/microC, and S/MMCS. It can be clearly observed that, in the S/mesoC cathode, orange polysulfides can be easily dissolved into the organic electrolyte solvent after only a few cycles and then diffused to the anode side, whereas for S/MMCS, benefiting from the physical barrier of the S/microC shell, the dissolution of polysulfides can be well restrained during cycles.

CONCLUSIONS

In summary, we have successfully synthesized a high-performance sulfur cathode *via* confining sulfur within a highly ordered meso-microporous core−shell carbon. This novel composite inherits the advantages of both highly ordered mesoporous carbon and microporous carbon. The mesoporous carbon "core" with high pore volume and highly ordered conductive channels can load adequate sulfur and facilitate complete redox reaction of the active material, while the microporous carbon "shell" with a strong adsorbing ability of polysulfides can maintain a stable cycle life. The S/MMCS composite exhibits a stable cycle performance

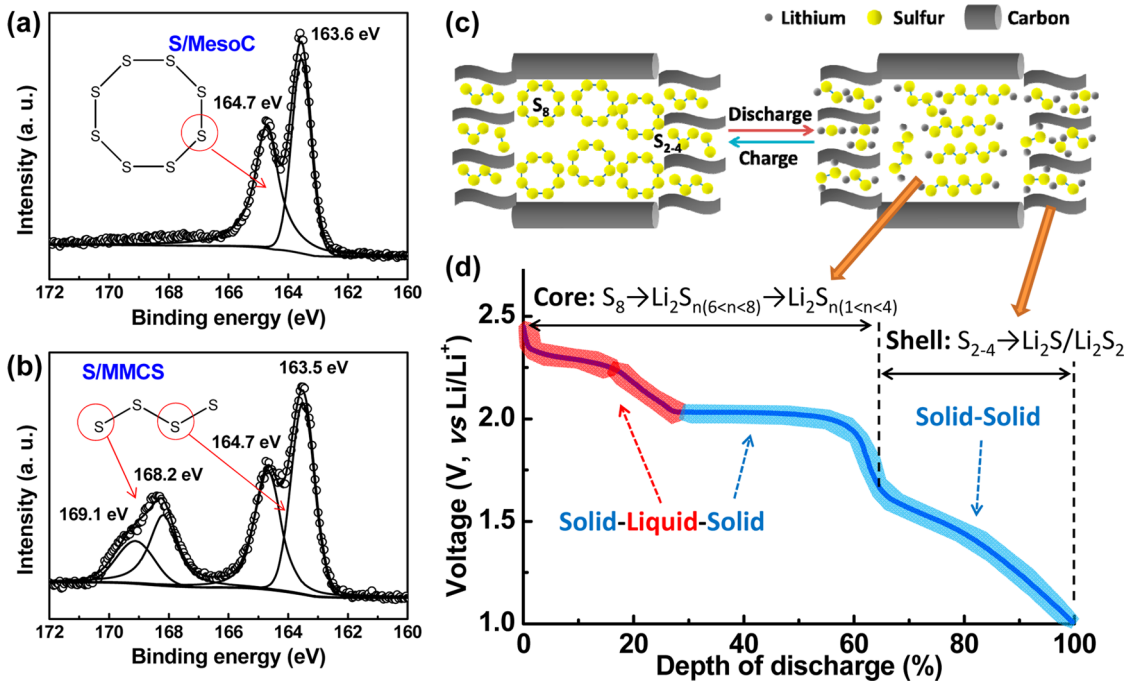

Figure 7. XPS spectra of S 2p for (a) S/mesoC and (b) S/MMCS. (c) A scheme of the S_8/mesoC-S_{2-4}/microC core−shell structure and the proposed (de)lithiation process inside the MMCS carbon structure. (d) A typical discharge profile and the corresponding electrochemical reactions of the S/MMCS electrode.

similar to S/microC without sacrificing sulfur loading, demonstrating that the diffusion of the polysulfides into the bulk electrolyte can be greatly reduced by the microC shell. Due to the availability of fabricating microporous carbon layers on the surface of mesoporous carbon *via* the above method, we believe that this strategy can inspire some other related novel materials with multilayers and hierarchical porous structures, which have great potential applications not only in energy conversion and storage but also in catalysis, adsorption, separation, drug delivery, sensors, and so on.

EXPERIMENTAL SECTION

Preparation of MMCS, MesoC, and MicroC. Highly ordered mesoporous SiO_2 (SBA-15) was prepared according to the previous report.[52] MMCS was fabricated by a modified nanocasting and surface-coating method. In a typical synthesis, 1.0 g of white powder of SBA-15 was ultrasonically dispersed into 5 mL f aqueous solution containing 1.25 g of sucrose and 0.14 g of H_2SO_4 in a glass beaker; the beaker was put into an oven and heated successively at 100 °C for 8 h and at 160 °C for another 8 h in air. The obtained brown powder was dispersed into 5 mL of aqueous solution containing 0.8 g of sucrose and 0.09 g of H_2SO_4 and then treated repeatedly as the above heating procedures. After that, 2.0 g of as-synthesized composite was dispersed in 100 mL of 1 mol L^{-1} H_2SO_4 containing 20 g of sucrose in a flask and refluxed at 120 °C for 24 h. The product was collected, dried at 80 °C, and carbonized at 900 °C for 5 h at Ar atmosphere. Finally, pure MMCS carbon was obtained by immersing the composite in a 10% hydrofluoric acid solution for 2 days to completely remove the SBA-15 template. For comparison, mesoC was fabricated by a classical nanocasting method with SBA-15 as hard template and sucrose as the carbon source.[53] MicroC was prepared by a hydrothermal method using sucrose as carbon source.[54] Both mesoC and microC were carbonized by the same procedure as MMCS.

Preparation of S/MMCS, S/MesoC, and S/MicroC composites. The S/MMCS composite was synthesized by a melting−diffusion strategy. Sulfur (0.6 g) was well mixed with 0.2 g of MMCS. The mixture was sealed in a Teflon pot and heated at 155 °C for 12 h. Then the composite was heated at 200 °C for 4 h under N_2 atmosphere to remove the sulfur outside of the porous carbon structure. After cooling to room temperature, the S/MMCS composite was obtained. The S/mesoC and S/microC composites were synthesized by the same method.

Characterization. XRD patterns were collected on X-ray powder diffraction (PANalytical X'pert PRO-DY2198, Holland) using Cu Kα radiation (λ = 0.15406 nm). SEM images were observed with Sirion 200 (FEI, Holland). TEM observation and the linear EDX elemental distribution were carried out with Tecnai G2 F30 (FEI, Holland). Raman spectra were measured by LabRAM HR800 (Horiba Jobin Yvon). Nitrogen sorption isotherms were obtained at −196 °C (77 K) with an ASAP 2020 (Micromeritics, US). The BET surface area was calculated from the adsorption data. The pore size distribution was calculated by the density functional theory (DFT) method from the adsorption branches of the isotherms. XPS measurements were performed on a Kratos Analytical spectrometer (AXIS ULTRA DLD-600W) using Al Kα (1486.6 eV) X-ray source. Sulfur contents of the carbon−sulfur composites were confirmed by TGA (PerkinElmer TGA7) in an Ar atmosphere with a heating rate of 10 °C min^{-1} from room temperature to 600 °C.

Electrochemical Measurements. To make the cathode, 80 wt % carbon/sulfur composite material, 10 wt % Super-P conductive carbon, 5 wt % styrene butadiene rubber (SBR), and 5 wt % carboxyl methyl cellulose sodium (NaCMC) were mixed in deionized water to form a homogeneous slurry, and then the slurry as spread onto a carbon-coated Al foil with the active material loading of about 1.0 mg cm^{-2}. The electrode film was dried in an oven at 80 °C overnight and then roll pressed and cut into round disks with a diameter of 8 mm. The 2032-type coin cells were assembled in a glovebox filled with Ar with Celgard

2300 membrane as separator and Li metal as anode. For S/MMCS and S/microC cathodes, the electrolyte was composed of 1 mol L^{-1} lithium bis(trifluoromethanesulfonyl)imide (LiTFSI) in a mixture of 1,3-dioxolane (DOL) and dimethoxymethane (DME) (v/v = 1:1), while for S/mesoC cathode, the electrolyte was added with 0.2 mol L^{-1} $LiNO_3$ to restrain the shuttle effect during cycling. The CV curves were recorded on an electrochemical workstation (CHI614b) at a scanning rate of 0.2 mV s^{-1} in the voltage range of 3.0−1.0 V. Galvanostatic discharge−charge tests were performed on a Land Battery Measurement System (Land, China) with cutoff voltages of 3.0−1.0 V. For long cycle test of S/mesoC as the control group, the cutoff voltages were set as 3.0−1.5 V to get a more stable performance. The current density was based on the weight of sulfur (1 C = 1680 mAh g^{-1}), and the capacities were calculated on the mass of sulfur and the total composites, respectively.

Conflict of Interest: The authors declare no competing financial interest.

Acknowledgment. This work was supported by the Natural Science Foundation of China (Grant Nos. 21273087, 21271078, and 51002057) and the PCSIRT (Program for Changjiang Scholars and Innovative Research Team in University). We thank the Analytical and Testing Center of HUST for XRD, FESEM, FTEM measurements and the State Key Laboratory of Materials Processing and Die & Mold Technology of HUST for TGA and TEM measurements.

Supporting Information Available: Additional figures. This material is available free of charge *via* the Internet at http://pubs.acs.org.

REFERENCES AND NOTES

1. Ji, X. L.; Nazar, L. F. Advances in Li−S Batteries. *J. Mater. Chem.* **2010**, *20*, 9821–9826.
2. Evers, S.; Nazar, L. F. New Approaches for High Energy Density Lithium−Sulfur Battery Cathodes. *Acc. Chem. Res.* **2013**, *46*, 1135–1143.
3. Manthiram, A.; Fu, Y.; Su, Y. S. Challenges and Prospects of Lithium−Sulfur Batteries. *Acc. Chem. Res.* **2013**, *46*, 1125–1134.
4. Yin, Y. X.; Xin, S.; Guo, Y. G.; Wan, L. J. Lithium−Sulfur Batteries: Electrochemistry, Materials, and Prospects. *Angew. Chem., Int. Ed.* **2013**, *52*, 13186–13200.
5. Patel, M. U.; Demir Cakan, R.; Morcrette, M.; Tarascon, J. M.; Gaberscek, M.; Dominko, R. Li−S Battery Analyzed by UV/Vis in Operando Mode. *ChemSusChem* **2013**, *6*, 1177–1181.
6. Walus, S.; Barchasz, C.; Colin, J. F.; Martin, J. F.; Elkaim, E.; Lepretre, J. C.; Alloin, F. New Insight into the Working Mechanism of Lithium−Sulfur Batteries: *In Situ* and Operando X-ray Diffraction Characterization. *Chem. Commun.* **2013**, *49*, 7899.
7. Barchasz, C.; Molton, F.; Duboc, C.; Lepretre, J. C.; Patoux, S.; Alloin, F. Lithium/Sulfur Cell Discharge Mechanism: An Original Approach for Intermediate Species Identification. *Anal. Chem.* **2012**, *84*, 3973–3980.
8. Seh, Z. W.; Li, W.; Cha, J. J.; Zheng, G.; Yang, Y.; McDowell, M. T.; Hsu, P. C.; Cui, Y. Sulphur-TiO_2 Yolk-Shell Nanoarchitecture with Internal Void Space for Long-Cycle Lithium−Sulphur Batteries. *Nat. Commun.* **2013**, *4*, 1331.
9. Li, W.; Zheng, G.; Yang, Y.; Seh, Z. W.; Liu, N.; Cui, Y. High-Performance Hollow Sulfur Nanostructured Battery Cathode through a Scalable, Room Temperature, One-step, Bottom-up Approach. *Proc. Natl. Acad. Sci. U.S.A.* **2013**, *110*, 7148–7153.
10. Guo, J.; Yang, Z.; Yu, Y.; Abruña, H. D.; Archer, L. A. Lithium-Sulfur Battery Cathode Enabled by Lithium-Nitrile Interaction. *J. Am. Chem. Soc.* **2013**, *135*, 763–767.
11. Zhou, G.; Pei, S.; Li, L.; Wang, D. W.; Wang, S.; Huang, K.; Yin, L. C.; Li, F.; Cheng, H. M. A Graphene-Pure-Sulfur Sandwich Structure for Ultrafast, Long-life Lithium-Sulfur Batteries. *Adv. Mater.* **2014**, *26*, 625–631.
12. Lin, Z.; Liu, Z.; Fu, W.; Dudney, N. J.; Liang, C. Lithium Polysulfidophosphates: A Family of Lithium-Conducting Sulfur-Rich Compounds for Lithium−Sulfur Batteries. *Angew. Chem., Int. Ed.* **2013**, *52*, 7460–7463.
13. Lee, K. T.; Black, R.; Yim, T.; Ji, X.; Nazar, L. F. Surface-Initiated Growth of Thin Oxide Coatings for Li-Sulfur Battery Cathodes. *Adv. Energy Mater.* **2012**, *2*, 1490–1496.
14. Su, Y. S.; Manthiram, A. Lithium−Sulphur Batteries with a Microporous Carbon Paper as a Bifunctional Interlayer. *Nat. Commun.* **2012**, *3*, 1166.
15. Wu, H. B.; Wei, S.; Zhang, L.; Xu, R.; Hng, H. H.; Lou, X. W. Embedding Sulfur in MOF-Derived Microporous Carbon Polyhedrons for Lithium−Sulfur Batteries. *Chem.—Eur. J.* **2013**, *19*, 10804–10808.
16. Wang, J.; Yao, Z.; Monroe, C. W.; Yang, J.; Nuli, Y. Carbonyl-β-Cyclodextrin as a Novel Binder for Sulfur Composite Cathodes in Rechargeable Lithium Batteries. *Adv. Funct. Mater.* **2013**, *23*, 1194–1201.
17. He, M.; Yuan, L. X.; Zhang, W. X.; Hu, X. L.; Huang, Y. H. Enhanced Cyclability for Sulfur Cathode Achieved by a Water-Soluble Binder. *J. Phys. Chem. C* **2011**, *115*, 15703–15709.
18. Xiao, L. F.; Cao, Y. L.; Xiao, J.; Schwenzer, B.; Engelhard, M. H.; Saraf, L. V.; Nie, Z. M.; Exarhos, G. J.; Liu, J. A Soft Approach to Encapsulate Sulfur: Polyaniline Nanotubes for Lithium-Sulfur Batteries with Long Cycle Life. *Adv. Mater.* **2012**, *24*, 1176–1181.
19. Mai, L. Q.; Minhas-Khan, A.; Tian, X. C.; Hercule, K. M.; Zhao, Y. L.; Lin, X.; Xu, X. Synergistic Interaction between Redox-active Electrolyte and Binder-free Functionalized Carbon for Ultrahigh Supercapacitor Performance. *Nat. Commun.* **2013**, *4*, 2923.
20. Zhao, Y. L.; Xu, L.; Mai, L. Q.; Han, C. H.; An, Q. Y.; Xu, X.; Liu, X.; Zhang, Q. J. Hierarchical Mesoporous Perovskite $La_{0.5}Sr_{0.5}CoO_{2.91}$ Nanowires with Ultrahigh Capacity for Li−Air Batteries. *Proc. Natl. Acad. Sci. U.S.A.* **2012**, *109*, 19569–19574.
21. Shi, Y.; Wan, Y.; Zhao, D. Ordered Mesoporous Non-oxide Materials. *Chem. Soc. Rev.* **2011**, *40*, 3854–3878.
22. Ji, X. L.; Lee, K. T.; Nazar, L. F. A Highly Ordered Nanostructured Carbon−Sulphur Cathode for Lithium-Sulphur Batteries. *Nat. Mater.* **2009**, *8*, 500–506.
23. Schuster, J.; He, G.; Mandlmeier, B.; Yim, T.; Lee, K. T.; Bein, T.; Nazar, L. F. Spherical Ordered Mesoporous Carbon Nanoparticles with High Porosity for Lithium−Sulfur Batteries. *Angew. Chem., Int. Ed.* **2012**, *51*, 3591–3595.
24. Weng, W.; Pol, V. G.; Amine, K. Ultrasound Assisted Design of Sulfur/Carbon Cathodes with Partially Fluorinated Ether Electrolytes for Highly Efficient Li/S Batteries. *Adv. Mater.* **2013**, *25*, 1608–1615.
25. Zhang, B.; Qin, X.; Li, G. R.; Gao, X. P. Enhancement of Long Stability of Sulfur Cathode by Encapsulating Sulfur into Micropores of Carbon Spheres. *Energy Environ. Sci.* **2010**, *3*, 1531–1537.
26. Xin, S.; Gu, L.; Zhao, N. H.; Yin, Y. X.; Zhou, L. J.; Guo, Y. G.; Wan, L. J. Smaller Sulfur Molecules Promise Better Lithium−Sulfur Batteries. *J. Am. Chem. Soc.* **2012**, *134*, 18510–18513.
27. Wei, S. C.; Zhang, H.; Huang, Y. Q.; Wang, W. K.; Xia, Y. Z.; Yu, Z. B. Pig Bone Derived Hierarchical Porous Carbon and Its Enhanced Cycling Performance of Lithium−Sulfur Batteries. *Energy Environ. Sci.* **2011**, *4*, 736–740.
28. Jayaprakash, N.; Shen, J.; Moganty, S. S.; Corona, A.; Archer, L. A. Porous Hollow Carbon@Sulfur Composites for High-Power Lithium-Sulfur Batteries. *Angew. Chem., Int. Ed.* **2011**, *50*, 5904–5908.
29. He, G.; Evers, S.; Liang, X.; Cuisinier, M.; Garsuch, A.; Nazar, L. F. Tailoring Porosity in Carbon Nanospheres for Lithium−Sulfur Battery Cathodes. *ACS Nano* **2013**, *7*, 10920–10930.
30. Zhang, C.; Wu, H. B.; Yuan, C.; Guo, Z.; Lou, X. W. D. Confining Sulfur in Double-Shelled Hollow Carbon Spheres for Lithium−Sulfur Batteries. *Angew. Chem., Int. Ed.* **2012**, *51*, 9592–9595.
31. Yao, H.; Zheng, G.; Li, W.; McDowell, M. T.; Seh, Z.; Liu, N.; Lu, Z.; Cui, Y. Crab Shells as Sustainable Templates from Nature for Nanostructured Battery Electrodes. *Nano Lett.* **2013**, *13*, 3385–3390.

32. Guo, J. C.; Xu, Y. H.; Wang, C. S. Sulfur-Impregnated Disordered Carbon Nanotubes Cathode for Lithium–Sulfur Batteries. *Nano Lett.* **2011**, *11*, 4288–4294.
33. Ji, L. W.; Rao, M. M.; Aloni, S.; Wang, L.; Cairns, E. J.; Zhang, Y. G. Porous Carbon Nanofiber–Sulfur Composite Electrodes for Lithium/Sulfur Cells. *Energy Environ. Sci.* **2011**, *4*, 5053–5059.
34. Chen, S.; Huang, X.; Liu, H.; Sun, B.; Yeoh, W.; Li, K.; Zhang, J.; Wang, G. 3D Hyperbranched Hollow Carbon Nanorod Architectures for High-Performance Lithium–Sulfur Batteries. *Adv. Energy Mater.* **2014**, *4*, DOI: 10.1002/aenm.201301761.
35. Zhou, G.; Yin, L. C.; Wang, D. W.; Li, L.; Pei, S.; Gentle, I. R.; Li, F.; Cheng, H. M. Fibrous Hybrid of Graphene and Sulfur Nanocrystals for High-performance Lithium–Sulfur Batteries. *ACS Nano* **2013**, *7*, 5367–5375.
36. Zhao, M. Q.; Liu, X. F.; Zhang, Q.; Tian, G. L.; Huang, J. Q.; Zhu, W.; Wei, F. Graphene/Single-Walled Carbon Nanotube Hybrids: One-Step Catalytic Growth and Applications for High-Rate Li–S Batteries. *ACS Nano* **2012**, *6*, 10759–10769.
37. Ji, L. W.; Rao, M. M.; Zheng, H. M.; Zhang, L.; Li, Y. C.; Duan, W. H.; Guo, J. H.; Cairns, E. J.; Zhang, Y. G. Graphene Oxide as a Sulfur Immobilizer in High Performance Lithium/Sulfur Cells. *J. Am. Chem. Soc.* **2011**, *133*, 18522–18525.
38. Huang, J. Q.; Liu, X. F.; Zhang, Q.; Chen, C. M.; Zhao, M. Q.; Zhang, S. M.; Zhu, W.; Qian, W. Z.; Wei, F. Entrapment of Sulfur in Hierarchical Porous Graphene for Lithium–Sulfur Batteries with High Rate Performance from −40 to 60°C. *Nano Energy* **2013**, *2*, 314–321.
39. Li, Z.; Yuan, L.; Yi, Z.; Liu, Y.; Xin, Y.; Zhang, Z.; Huang, Y. A Dual Coaxial Nanocable Sulfur Composite for High-Rate Lithium–Sulfur Batteries. *Nanoscale* **2014**, *6*, 1653–1660.
40. Zhao, M. Q.; Zhang, Q.; Huang, J. Q.; Tian, G. L.; Nie, J. Q.; Peng, H. J.; Wei, F. Unstacked Double-Layer Templated Graphene for High-Rate Lithium–Sulphur Batteries. *Nat. Commun.* **2014**, *5*, 3410.
41. Lee, J. T.; Zhao, Y.; Thieme, S.; Kim, H.; Oschatz, M.; Borchardt, L.; Magasinski, A.; Cho, W. I.; Kaskel, S.; Yushin, G. Sulfur-Infiltrated Micro- and Mesoporous Silicon Carbide-Derived Carbon Cathode for High-Performance Lithium Sulfur Batteries. *Adv. Mater.* **2013**, *25*, 4573–4579.
42. Lu, S.; Cheng, Y.; Wu, X.; Liu, J. Significantly Improved Long-Cycle Stability in High-Rate Li-S Batteries Enabled by Coaxial Graphene Wrapping over Sulfur-Coated Carbon Nanofibers. *Nano Lett.* **2013**, *13*, 2485–2489.
43. Zhang, J.; Ye, H.; Yin, Y.; Guo, Y. Core-shell Meso/Microporous Carbon Host for Sulfur Loading toward Applications in Lithium-Sulfur Batteries. *J. Energy Chem.* **2014**, *23*, 308–314.
44. Zhang, Z.; Li, Z.; Hao, F.; Wang, X.; Li, Q.; Qi, Y.; Fan, R.; Yin, L. 3D Interconnected Porous Carbon Aerogels as Sulfur Immobilizers for Sulfur Impregnation for Lithium–Sulfur Batteries with High Rate Capability and Cycling Stability. *Adv. Funct. Mater.* **2014**, *24*, 2500–2509.
45. Xin, S.; Yin, Y. X.; Wan, L. J.; Guo, Y. G. Encapsulation of Sulfur in a Hollow Porous Carbon Substrate for Superior Li–S Batteries with Long Lifespan. *Part. Part. Sys. Char.* **2013**, *30*, 321–325.
46. Wang, D. W.; Zhou, G.; Li, F.; Wu, K. H.; Lu, G. Q.; Cheng, H. M.; Gentle, I. R. A Microporous-Mesoporous Carbon with Graphitic Structure for a High-Rate Stable Sulfur Cathode in Carbonate Solvent-based Li–S Batteries. *Phys. Chem. Chem. Phys.* **2012**, *14*, 8703–8710.
47. Li, Z.; Yuan, L.; Yi, Z.; Sun, Y.; Liu, Y.; Jiang, Y.; Shen, Y.; Xin, Y.; Zhang, Z.; Huang, Y. Insight into the Electrode Mechanism in Lithium–Sulfur Batteries with Ordered Microporous Carbon Confined Sulfur as the Cathode. *Adv. Energy Mater.* **2014**, *4*, DOI: 10.1002/aenm.201301473.
48. Li, G. C.; Li, G. R.; Ye, S. H.; Gao, X. P. A Polyaniline-Coated Sulfur/Carbon Composite with an Enhanced High-Rate Capability as a Cathode Material for Lithium/Sulfur Batteries. *Adv. Energy Mater.* **2012**, *2*, 1238–1245.
49. Wu, F.; Chen, J.; Li, L.; Zhao, T.; Chen, R. Improvement of Rate and Cycle Performence by Rapid Polyaniline Coating of a MWCNT/Sulfur Cathode. *J. Phys. Chem. C* **2011**, *115*, 24411–24417.
50. Yang, Y.; Yu, G. H.; Cha, J. J.; Wu, H.; Vosgueritchian, M.; Yao, Y.; Bao, Z. A.; Cui, Y. Improving the Performance of Lithium-Sulfur Batteries by Conductive Polymer Coating. *ACS Nano* **2011**, *5*, 9187–9193.
51. Zhang, W.; Qiao, D.; Pan, J.; Cao, Y.; Yang, H.; Ai, X. A Li^+-Conductive Microporous Carbon-Sulfur Composite for Li-S Batteries. *Electrochim. Acta* **2013**, *87*, 497–502.
52. Ji, X.; Evers, S.; Black, R.; Nazar, L. F. Stabilizing Lithium–Sulphur Cathodes Using Polysulphide Reservoirs. *Nat. Commun.* **2011**, *2*, 325.
53. Jun, S.; Joo, S. H.; Ryoo, R.; Kruk, M.; Jaroniec, M.; Liu, Z.; Ohsuna, T.; Terasaki, O. Synthesis of New, Nanoporous Carbon with Hexagonally Ordered Mesostructure. *J. Am. Chem. Soc.* **2000**, *122*, 10712–10713.
54. Hassoun, J.; Kim, J.; Lee, D. J.; Jung, H. G.; Lee, S. M.; Sun, Y. K.; Scrosati, B. A Contribution to the Progress of High Energy Batteries: A Metal-free, Lithium-ion, Silicon–Sulfur battery. *J. Power Sources* **2012**, *202*, 308–313.